CHEMISTRY

Reconstruction of the time-dependent electronic wave packet arising from molecular autoionization

Roger Y. Bello[1], Sophie E. Canton[2,3], Denis Jelovina[1], John D. Bozek[4], Bruce Rude[5], Olga Smirnova[6,7], Mikhail Y. Ivanov[6,8,9], Alicia Palacios[1,10], Fernando Martín[1,11,12]*

Autoionizing resonances are paradigmatic examples of two-path wave interferences between direct photoionization, which takes a few attoseconds, and ionization via quasi-bound states, which takes much longer. Time-resolving the evolution of these interferences has been a long-standing goal, achieved recently in the helium atom owing to progress in attosecond technologies. However, already for the hydrogen molecule, similar time imaging has remained beyond reach due to the complex interplay between fast nuclear and electronic motions. We show how vibrationally resolved photoelectron spectra of H_2 allow one to reconstruct the associated subfemtosecond autoionization dynamics by using the ultrafast nuclear dynamics as an internal clock, thus forgoing ultrashort pulses. Our procedure should be general for autoionization dynamics in molecules containing light nuclei, which are ubiquitous in chemistry and biology.

INTRODUCTION

The decay of quasi-bound (resonant) states immersed in the continuum of many-particle systems is one of the most common manifestations of intrinsic two-way interferences in physics (*1*–*4*). In atoms, these states generally show up as asymmetric peaks in photoabsorption spectra recorded as a function of photon energy (*5*, *6*). The origin of the asymmetry is the interference between the two processes that lead to the same photoelectron energy: direct ionization, which is a fast, almost instantaneous process, and autoionization, which is much slower and typically occurs on a time scale of few femtoseconds to few tens of femtoseconds. As shown by Fano in the early 1960s (*6*), the shape of the resonant peaks, $\sigma(E)$, is completely determined by the resonance position, E_r, the autoionization width, Γ (that is, the inverse of the resonance lifetime), and the so-called resonant profile (or Fano) parameter, q, through the well-known formula $\sigma(E) = \sigma_0(q + \epsilon)^2/(1 + \epsilon^2)$, where $\epsilon = 2(E - E_r)/\Gamma$ and σ_0 is the total nonresonant background cross section.

Although first observed in the photoionization of rare gases (*5*), Fano profiles are not exclusive to atomic systems. They are also found in photoionization spectra of simple molecules (N_2, CO, etc.) (*7*, *8*), in scanning tunneling spectra of magnetic impurities lying on metal surfaces (Kondo effect) (*9*–*11*), in plasmonic systems (*12*) and optical metamaterials (*13*, *14*), in photonic (*15*, *16*) and phononic crystals (*17*, *18*), and in matter-wave scattering in Bose-Einstein (*19*, *20*) and Fermi gases (*21*), to name a few examples. In all cases, the origin of the asymmetry is similar to that in atoms: the interference between a fast and a slow process leading to the same final state.

As a consequence of the delay between the direct (fast) and the resonant (slow) processes, the interference takes time to fully set up and can be controlled. With the advent of attosecond techniques (*22*), it has recently been possible to monitor the birth and subsequent evolution of the electronic wave packets generated by atomic resonances during photoionization of He and hence to visualize the buildup of the Fano profiles with subfemtosecond time resolution (*23*, *24*). This work has opened the door to the control of electron dynamics in atoms by acting on the time scale inherent to electronic motion.

However, when it comes to H_2, the prototype molecular system, the situation is much more complex. First, the slow component of the electron dynamics associated with autoionization occurs on the same few-femtosecond time scale as the fast nuclear dynamics associated with the proton motion so that the usual Fano picture is no longer applicable (*25*). As a consequence, the photoionization spectra show no clear trace of resonant features (*26*–*28*). Second, the coupling of the electronic and nuclear motions entangles, in a quantum mechanical manner, the photoelectron with the molecular ion, scrambling the interference pattern if the ionic state is not measured. To uncover the interference, experiments have looked at the dissociative ionization ($H_2 \rightarrow H + H^+ + e^-$) (*29*–*32*) or radiative ($H_2 \rightarrow H + H + h\nu$) channels (*33*, *34*), which, however, only account for less than a few percent of the total photoionization cross section. The need to measure the photoelectron, together with the energy of the emitted photon or of the dissociating fragments (ideally, in coincidence, to fully access correlations between electronic and nuclear motions), reduces the signal even further.

These factors have prevented time-resolved studies of H_2 autoionization. Currently available attosecond pulses, which are required to provide the necessary time resolution, are too weak to obtain dissociative ionization spectra in coincidence. A similarly challenging scenario is expected for most organic and biological molecules, because they contain a significant proportion of hydrogen atoms.

The difficulty would be very much alleviated if one could extract time-resolved information from the dominant nondissociative channel. Although no resonance features are visible in the total nondissociative photoionization spectra of H_2, theory has long ago predicted (*28*) that photoionization spectra in which the vibrational state of the remaining H_2^+ ion is resolved (hereafter called v-spectra) do show resonance

[1]Departamento de Química, Módulo 13, Universidad Autónoma de Madrid, 28049 Madrid, Spain. [2]Extreme Light Infrastructure Attosecond Light Pulse Source, ELI-HU Non-Profit Ltd., Dugonics ter 13, Szeged 6720, Hungary. [3]Attosecond Science Group, Deutsches Elektronen-Synchrotron (DESY), Notkestrasse 85, D-22607 Hamburg, Germany. [4]Synchrotron SOLEIL, L'Orme des Merisiers, Saint-Aubin, BP 48, 91192 Gif-sur-Yvette Cedex, France. [5]Advanced Light Source, Lawrence Berkeley National Laboratory, Berkeley, CA 94720, USA. [6]Max-Born Institute for Nonlinear Optics and Short Pulse Spectroscopy, Max-Born-Straße 2A, D-12489 Berlin, Germany. [7]Technische Universität Berlin, Ernst-Ruska-Gebäude, Hardenbergstr. 36 A, 10623 Berlin, Germany. [8]Department of Physics, Imperial College London, South Kensington Campus, SW72AZ London, UK. [9]Institute of Physics, Humboldt University Berlin, Newtonstrasse 15, 12489 Berlin, Germany. [10]Institute for Advanced Research in Chemical Sciences, Universidad Autónoma de Madrid, 28049 Madrid, Spain. [11]Instituto Madrileño de Estudios Avanzados en Nanociencia, Cantoblanco, 28049 Madrid, Spain. [12]Condensed Matter Physics Center (IFIMAC), Universidad Autónoma de Madrid, 28049 Madrid, Spain.
*Corresponding author. Email: fernando.martin@uam.es

features associated with the H_2 doubly excited states (although they vanish when summing over all H_2^+ vibrational states). Furthermore, it has been recently demonstrated (*35*) that these v-spectra provide a time-energy mapping of autoionization dynamics. Ultrafast nuclear motion is the clock that maps these dynamics into the final population of the bound vibrational states of H_2^+, allowing one to image H_2 autoionization without the need for ultrashort probe pulses as are used in current attosecond pump-probe experiments (*36*). That is, nuclear motion can act as an internal probe of the ultrafast electron dynamics triggered by the ionizing field.

Although v-spectra have been measured for many molecules over a wide range of photon energies (*37*–*42*), in the case of H_2, they have only been recorded at high photon energies (*37*). Therefore, there is no experimental evidence so far that H_2 resonance structures can be resolved in the dominant nondissociative channel, thus remaining one of the fundamental unsolved problems in molecular photoionization.

Here, we report accurate synchrotron radiation measurements of the vibrationally resolved photoionization cross sections of H_2 and show that they exhibit the signature of autoionizing states. We fully resolve the shape of their corresponding resonant features and find them to be in excellent agreement with nearly exact theoretical calculations. We then fully reconstruct the autoionization dynamics and the buildup of the interference between direct ionization and autoionization in H_2 with subfemtosecond time resolution.

RESULTS AND DISCUSSION

Figure 1 shows the measured and calculated vibrationally resolved photoionization cross sections referred to the dominant ionization channel $H_2 + h\nu \rightarrow H_2^+(v = 2) + e^-$ (in short, v-ratios). The measured photoelectron spectra from which these ratios have been extracted are presented in section S1. Very prominent features with distinct profiles are observed for photon energies between 24 and 37 eV, in clear contrast to the featureless vibrationally unresolved photoionization cross sections in the same range of photon energies. Following earlier theoretical work (*43*, *44*), we assign the observed structures to autoionization from the lowest $Q_1\ ^1\Sigma_u^+$ and $Q_2\ ^1\Pi_u$ doubly excited states of H_2. The corresponding potential energy curves are shown in Fig. 2. These states lie above the first ($1s\sigma_g$) and the second ($2p\sigma_u$) ionization thresholds of H_2, respectively, and can therefore decay by directly emitting an electron and leaving H_2^+ in the ground electronic state $1s\sigma_g$. Decay of Q_2 states can also be accompanied by excitation of the remaining electron to the $2p\sigma_u$ excited state of H_2^+, which is entirely repulsive and therefore does not contribute to the nondissociative ionization channel. As the autoionization decay takes a few femtoseconds, the nuclei have enough time to move along the corresponding repulsive potential energy curves before the electron is emitted (see the red and blue paths shown in Fig. 2). As a consequence, the populated doubly excited states can efficiently ionize over a wide range of internuclear distances, from the Franck-Condon region up to well outside this region, thus leading to a broad distribution of $H_2^+(1s\sigma_g)$ vibrational states. In general, the slower the autoionization, the higher the vibrational state in which H_2^+ is left, because the rapidly evolving nuclear wave packet in momentum space can more efficiently overlap with higher vibrational states of $H_2^+(1s\sigma_g)$ (*35*). Therefore, by vibrationally resolving the final state of the remaining H_2^+ ion, one gains access to the dynamics of the autoionization decay: The nuclear motion acts as an internal clock that can be used to extract dynamical information about this decay.

The time evolution of the autoionizing electron wave packet can be retrieved by using an extension of the Fano formalism that incorporates the effect of the nuclear motion on an equal footing with electronic motion. In this formalism, molecular rotation is not taken into account because it is orders of magnitude slower than autoionization (picoseconds versus femtoseconds) so that the orientation barely changes

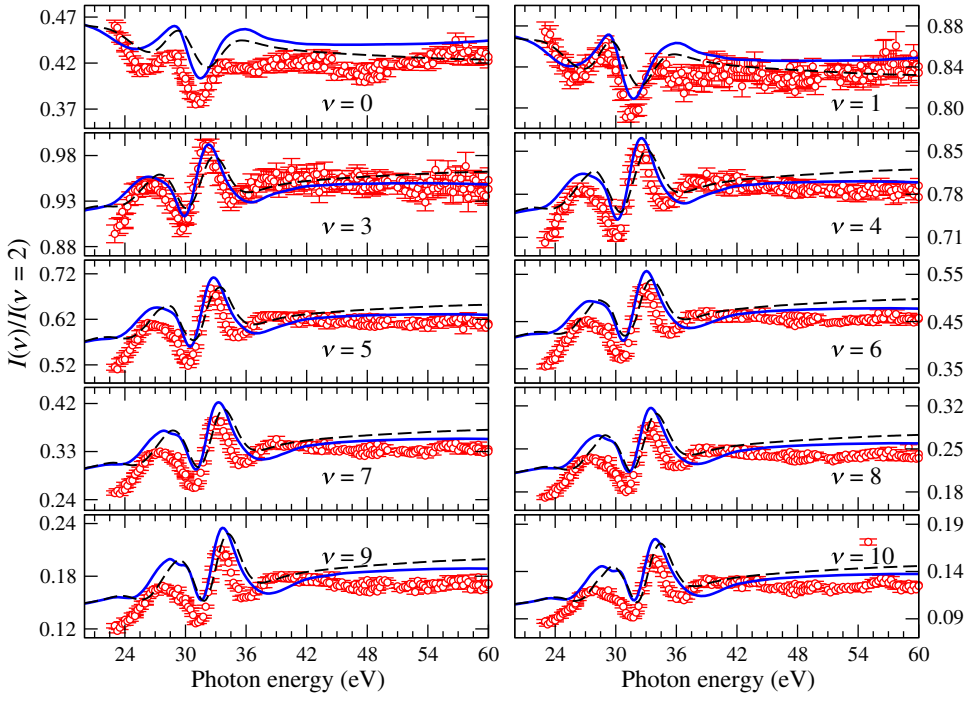

Fig. 1. Vibrationally resolved photoionization cross sections normalized to that for the $v = 2$ state of H_2^+ as a function of photon energy. Circles with error bars: Experimental data. Full lines: Ab initio calculation. Dashed lines: Fit to the experimental data by using the extended Fano model described in the text [see also (*35*)].

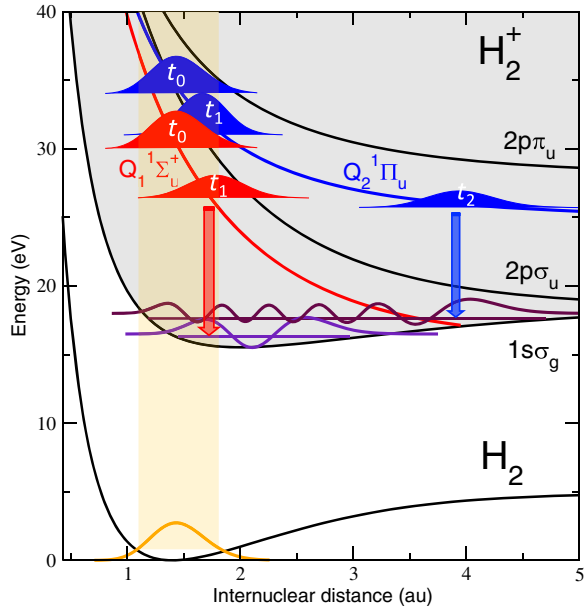

Fig. 2. Evolution of the nuclear wave packets generated in the H_2 doubly excited states by the XUV radiation. The nuclear wave packets follow the potential energy curves of the Q_1 and Q_2 states until the latter autoionizes by emitting an electron and leaving the H_2^+ cation in the $1s\sigma_g$ electronic state. The longer the autoionization time, the longer the wave packet travels in the *Q* states and the higher the vibrational state in which H_2^+ is left after autoionization, because the overlap between the moving nuclear wave packet and the final vibrational state is only efficient near the classical turning points of the latter. The Franck-Condon region where the transition from the ground state to the continuum takes place is indicated by a shadowed orange area.

during the electron emission process. The resonant contribution to the photoelectron wave packet correlated to the v-state of the H_2^+ cation can be approximately written (*35*)

$$|\psi_v(\epsilon,t)|^2 = C\sqrt{\sigma_v^0(\epsilon)}\int_0^t dt'\cos[(E_v+\epsilon)t']\int dR\chi_v(R)\sqrt{\frac{\Gamma(R)}{2\pi}}\chi_Q(R,t') \quad (1)$$

where *C* is a constant, $\sigma_v^0(\epsilon)$ is the nonresonant background cross section, ϵ is the energy of the emitted electron, *R* is the internuclear distance, χ_v is the final vibrational state of H_2^+ with vibronic (electronic plus vibrational) energy E_v, Γ is the autoionization width of the *Q* resonance, and χ_Q is the nuclear wave packet evolving along the potential energy curve of this resonance, described within the semiclassical WKB approximation [see, for example, (*45*) for an introduction to WKB]. We note that, for each final vibrational state of H_2^+, the photoelectron energy and the photon energy *E* are related by the formula $E + E_g = E_v + \epsilon$, where E_g is the H_2 ground-state energy. The measured resonant profile $\sigma_v(\epsilon)$ is given by $\sigma_v(\epsilon) = |\psi_v(\epsilon, t = \infty)|^2$. The validity of this model has been demonstrated in (*35*). The key unknown quantity of interest in Eq. 1 is $\Gamma(R)$, which encodes the coupled electron-nuclear autoionization. Here, we have used Eq. 1 for $t = \infty$ to fit the measured photoionization cross sections, considering $\Gamma(R)$ as a free parametric function. The results of such a fit, for the lowest $Q_1\ ^1\Sigma_u^+$ and $Q_2\ ^1\Pi_u$ doubly excited states, are shown as dashed lines in Fig. 1. The agreement with ab initio theory and experiment is excellent. The details of the fitting procedure can be found in the Supplementary Materials.

Now, using the experimentally determined $\Gamma(R)$ function and Eq. 1, we have thus reconstructed the electronic wave packet generated at different times *t* in the vicinity of each resonance. This procedure resembles that followed by Gruson *et al.* (*23*) in the He atom, except for the fact that the present reconstruction formula incorporates the effect of the nuclear dynamics, which is essential to correctly account for the phase evolution of the molecular electronic wave packet. The other important difference is that, here, the phase information is not retrieved by using an ultrashort light pulse but from the internal probe provided by the nuclear motion. The results of this reconstruction procedure for the $Q_1\ ^1\Sigma_u^+$ and $Q_2\ ^1\Pi_u$ resonances are shown in Fig. 3, where they are compared with the actual electron wave packet densities obtained from the ab initio calculations. As can be seen, the time evolution of the reconstructed and calculated wave packet densities is very similar, thus demonstrating that one can obtain accurate amplitude and phase information about the autoionizing electronic wave packet from the vibrationally resolved measurements performed over a wide range of photon energies and with sufficient energy resolution to access all the resonant features. It is important to emphasize that, because of the dipole selection rule that operates under the present experimental conditions, the $Q_1\ ^1\Sigma_u^+$ and $Q_2\ ^1\Pi_u$ reconstructions correspond to the actual wave packets resulting from molecules oriented parallel and perpendicular to the polarization direction of the synchrotron radiation field, respectively.

Figure 3 shows that both wave packets experience marked changes during the first femtosecond, with the appearance of more and more nodes as time goes by. Subsequently, some of the nodes disappear, and after around 3 fs, no more significant changes take place. Therefore, all the interferences resulting from the coupled electron and nuclear dynamics associated with the autoionization decay set up in less than 3 fs. One can now compare these results with those recently obtained for the $2s2p\ ^1P^o$ resonance of He (*23*), to which the $Q_1\ ^1\Sigma_u^+$ and $Q_2\ ^1\Pi_u$ resonances correlate in the united atom limit ($R = 0$). A noticeable difference with the atomic case is that the calculated ionization rate profiles do not follow the standard Fano picture because they exhibit at least two maxima and two minima (even more at very short times). This is the consequence of the coupling between the electronic and the nuclear motion, absent in atoms. Another interesting result is that the evolutions of the $Q_1\ ^1\Sigma_u^+$ and $Q_2\ ^1\Pi_u$ wave packets are different, which is due to the different values of the corresponding autoionization widths $\Gamma(R)$ and their different variation with internuclear distance. As pointed out in early work (*43*, *44*), the autoionization width for the $Q_1\ ^1\Sigma_u^+$ resonance is larger than that for the $Q_2\ ^1\Pi_u$ resonance. As a consequence, interferences in the $Q_1\ ^1\Sigma_u^+$ wave packet evolve faster and the stationary regime is reached earlier.

The weak features observed in the calculated Σ wave packet at around 20 eV, a region that is not accessible in the present experiment, are most likely due to the crossing of the potential energy curve of the Q_1 doubly excited state with the ionization threshold, which occurs at an internuclear distance of about 4 atomic units (au; see Fig. 2). Similar features are not observed in the Π wave packet, because the Q_2 potential energy curve does not cross the threshold.

CONCLUSION AND PERSPECTIVES

In summary, we have been able to identify the long-awaited signature of H_2 doubly excited states in the nondissociative photoionization channel and then to reconstruct the subfemtosecond time evolution of the molecular electronic wave packet in the vicinity of the lowest $Q_1\ ^1\Sigma_u^+$ and $Q_2\ ^1\Pi_u$ doubly excited states. Both the time resolution and the phase

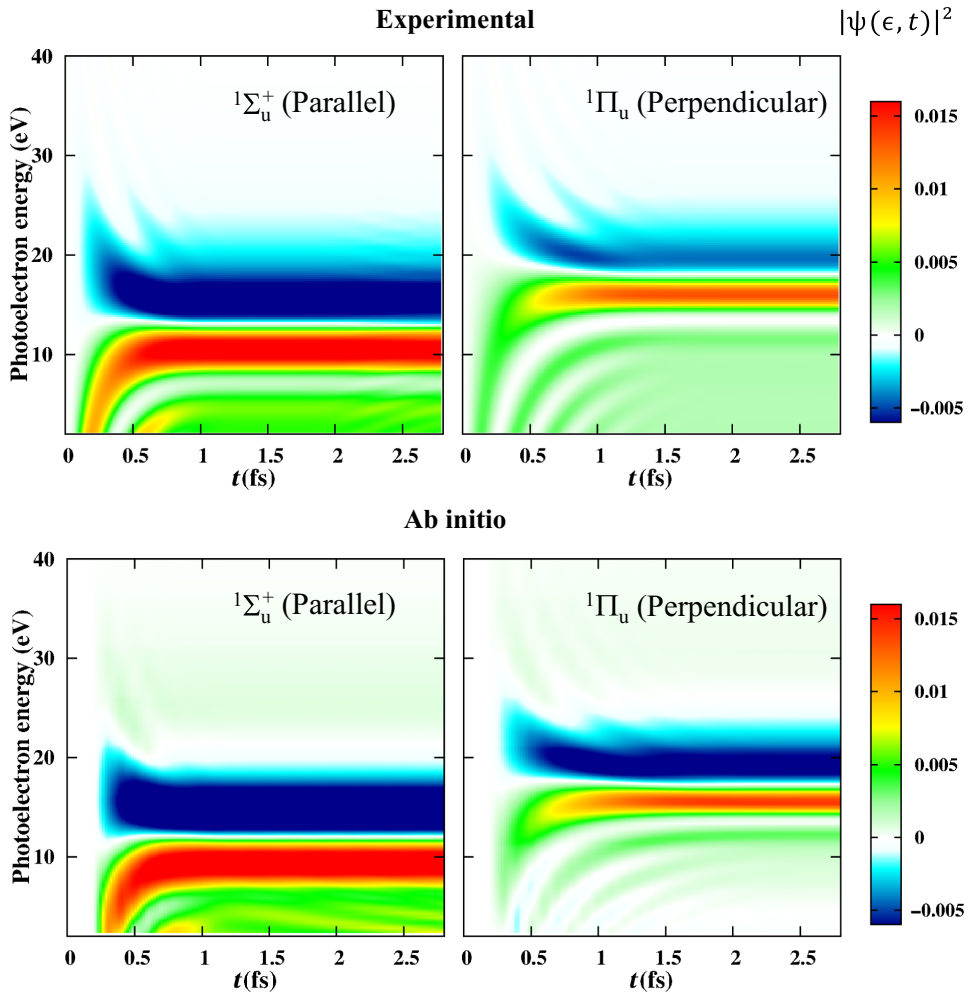

Fig. 3. Buildup in time of the interference between direct ionization and autoionization from the lowest Q_1 $^1\Sigma_u^+$ (left panels) and Q_2 $^1\Pi_u$ (right panels) doubly excited states corresponding to the $v = 5$ vibrational state of the remaining H_2^+ ion. Similar plots can be obtained for other final v's. (**Top**) Square of the wave packet densities obtained from experiment as a function of photoelectron energy (y axis) and time (x axis). (**Bottom**) Results of the ab initio calculations for a pulse of 200 as. For a better visualization, the monotonic decreasing background associated with the direct ionization channel has been subtracted in all cases.

information necessary for the reconstruction are imprinted in the nuclear motion that follows the excitation by the extreme ultraviolet (XUV) field. The nuclear dynamics act as an internal probe of the system, in contrast to the usual pump-probe schemes where the probing is performed by using an (external) ultrashort pulse. For the reconstruction to be experimentally feasible, one must have some a priori knowledge of the molecular system under investigation, namely, of the potential energy curves (surfaces) of the ground and quasi-bound states embedded in the continuum, from which the vibrational wave functions can be estimated. In general, this is no longer a daunting task for small- and medium-sized molecules, because a plethora of user-friendly quantum chemistry packages for bound state calculations can provide this information with high accuracy. In addition, vibrationally resolved photoelectron spectra of small polyatomic molecules can be routinely accessed in most synchrotrons. With these generally available tools, one can retrieve from experiment the autoionization width as a function of the molecular geometry using a simple semiclassical analysis and hence reconstruct the time-dependent wave packet.

The core idea of our method should be applicable to any molecule containing hydrogen atoms because they move fast and therefore can be used as an internal clock of the system. Measuring vibrationally resolved photoelectron spectra of molecules with high-energy resolution can be routinely achieved at synchrotrons, so they could be used as complementary tools to attosecond and few-femtosecond pump-probe techniques to obtain dynamical information on the ultrafast autoionization or Auger decay of molecules. Furthermore, by performing isotopic substitution, for example, by replacing atomic hydrogen with deuterium, one could also exert some control on the timing of the autoionization decay, because the nuclear mass determines the velocity of the nuclear wave packet that is created. Implementation of the present reconstruction method in more complex hydrogen-containing molecules, such as water or ammonia, should be the next step toward understanding autoionization dynamics in molecules of chemical interest.

MATERIALS AND METHODS

Experimental methods

The experiments were performed at the high-resolution beamline 10 of the Advanced Light Source. Effusive molecular beams were ionized by

linearly polarized radiation. The photoelectron spectra were measured using a Scienta SES-200 hemispherical analyzer (*46*) at 54.7° with respect to the light polarization axis (eliminating angular effects) and were corrected afterward for spectrometer transmission. Because of the high performance of the analyzer, the vibrational lines were kept resolved throughout the photon energy range covered (22 to 60 eV). With negligible stray background, reliable areas proportional to the cross sections were extracted by summing the counts in a given kinetic energy window, avoiding systematic uncertainties attached to baselines coming from overlapping peaks and bypassing recourse to fitting with analytical line shapes. This was particularly important for these experiments because of the underlying rotational structure, almost resolved for the low v and responsible for asymmetric broadening for the high v.

Ab initio calculations

The theoretical method accounted for electron correlation and interferences between the different ionization and dissociative channels to obtain the electronic and vibrational wave functions of H_2. It made use of B-spline functions and was successfully applied to study a variety of ionization problems in H_2, such as resonant dissociative photoionization induced by synchrotron radiation or ultrashort pulses (*36*, *47*). We refer the reader to those works and, for more details, to the reviews of (*48*–*50*). The specific details for the present calculations are given below.

Vibrationally resolved photoionization cross sections were obtained by using first-order perturbation theory. The final wave function, a solution of the time-dependent Schrödinger equation, was expanded in a basis set of Born-Oppenheimer states, written as products of electronic and nuclear wave functions. In this expansion, the bound electronic states of H_2 were obtained by performing a configuration interaction calculation in a basis of antisymmetrized products of one-electron H_2^+ functions, and the electronic continuum states were obtained by solving the multichannel scattering equations in a basis of uncoupled continuum states that are written as products of a one-electron wave function for the bound electron and an expansion on spherical harmonics and B-spline functions for the continuum electron. The multichannel expansion includes the two lowest ionic states ($1s\sigma_g$ and $2p\sigma_u$) and partial waves for the emitted electron up to a maximum angular momentum $l_{max} = 7$ enclosed in a box of 60 au. The one-electron orbitals for the bound electron were consistently computed in the same radial box using single-center expansions with corresponding angular momenta up to $l_{max} = 16$. All electronic wave functions were evaluated in a grid of internuclear distances in the interval $R = 0.1$ to 12 au. The corresponding nuclear vibrational and dissociative wave functions were obtained by diagonalizing the nuclear Schrödinger equation for all electronic states included in the expansion over Born-Oppenheimer states. This expansion includes the six lowest electronically bound states, the six lowest doubly excited states of the Q_1 and Q_2 resonance series, and the electronic continuum states associated to the $1s\sigma_g$ and $2p\sigma_u$ ionization thresholds, all of them for both $^1\Sigma_u^+$ and $^1\Pi_u$ symmetries. Couplings between these states induced by the H_2 Hamiltonian and between these states and the $X^1\Sigma_g^+$ ground state of H_2 induced by the linearly polarized XUV radiation field were explicitly evaluated.

SUPPLEMENTARY MATERIALS

Supplementary material for this article is available at http://advances.sciencemag.org/cgi/content/full/4/8/eaat3962/DC1

Section S1. Measured photoelectron spectra

Section S2. Validity and limitations of the reconstruction model

Section S3. Fit to the experimental data

Fig. S1. Measured photoelectron spectra as a function of photon and binding energies.

Fig. S2. Same as in fig. S1 but now with spectra obtained at different photon energies overlaying.

Fig. S3. Comparison between the experimental and fitted photoionization cross sections for $v = 3$.

Reference (*51*)

REFERENCES AND NOTES

1. N. Bohr, in *The Library of Living Philosophers, Volume 7. Albert Einstein: Philosopher-Scientist*, P. A. Schilpp, Ed. (Open Court, 1949), pp. 199–241.
2. R. H. Brown, R. Q. Twiss, Correlation between photons in two coherent beams of light. *Nature* **177**, 27–29 (1956).
3. G. Jaeger, A. Shimony, L. Vaidman, Two interferometric complementarities. *Phys. Rev. A* **51**, 54–67 (1995).
4. K. P. Zetie, S. F. Adams, R. M. Tocknell, How does a Mach-Zehnder interferometer work? *Phys. Educ.* **35**, 46 (2000).
5. H. Beutler, Über Absorptionsserien von Argon, Krypton und Xenon zu Termen zwischen den beiden Ionisierungsgrenzen $^2P_{3}{}^{2/0}$ und $^2P_{1}{}^{2/0}$. *Zeitschrift für Phys.* **93**, 177–196 (1935).
6. U. Fano, Effects of configuration interaction on intensities and phase shifts. *Phys. Rev.* **124**, 1866–1878 (1961).
7. M. Eckstein, C.-H. Yang, F. Frassetto, L. Poletto, G. Sansone, M. J. J. Vrakking, O. Kornilov, Direct imaging of transient Fano resonances N_2 using time-, energy-, and angular-resolved photoelectron spectroscopy. *Phys. Rev. Lett.* **116**, 163003 (2016).
8. J. J. Hopfield, Absorption and emission spectra in the region λ 600–1100 nm. *Phys. Rev.* **35**, 1133–1134 (1930).
9. V. Madhavan, W. Chen, T. Jamneala, M. F. Crommie, N. S. Wingreen, Tunneling into a single magnetic atom: Spectroscopic evidence of the Kondo resonance. *Science* **280**, 567–569 (1998).
10. A. R. Schmidt, M. H. Hamidian, P. Wahl, F. Meier, A. V. Balatsky, J. D. Garrett, T. J. Williams, G. M. Luke, J. C. Davis, Imaging the Fano lattice to 'hidden order' transition in URu_2Si_2. *Nature* **465**, 570–576 (2010).
11. M. Garnica, D. Stradi, S. Barja, F. Calleja, C. Díaz, M. Alcamí, N. Martín, A. L. Vázquez de Parga, F. Martín, R. Miranda, Long-range magnetic order in a purely organic 2D layer adsorbed on epitaxial graphene. *Nat. Phys.* **9**, 368–374 (2013).
12. J. A. Fan, C. Wu, K. Bao, J. Bao, R. Bardhan, N. J. Halas, V. N. Manoharan, P. Nordlander, G. Shvets, F. Capasso, Self-assembled plasmonic nanoparticle clusters. *Science* **328**, 1135–1138 (2010).
13. V. A. Fedotov, M. Rose, S. L. Prosvirnin, N. Papasimakis, N. I. Zheludev, Sharp trapped-mode resonances in planar metamaterials with a broken structural symmetry. *Phys. Rev. Lett.* **99**, 147401 (2007).
14. B. Luk'yanchuk, N. I. Zheludev, S. A. Maier, N. J. Halas, P. Nordlander, H. Giessen, C. Tow Chong, The Fano resonance in plasmonic nanostructures and metamaterials. *Nat. Mater.* **9**, 707–715 (2010).
15. S. Fan, J. D. Joannopoulos, Analysis of guided resonances in photonic crystal slabs. *Phys. Rev. B.* **65**, 235112 (2002).
16. C. Lin, Z. Lu, S. Shi, G. Jin, D. W. Prather, Experimentally demonstrated filters based on guided resonance of photonic-crystal films. *Appl. Phys. Lett.* **87**, 91102 (2005).
17. L. Chen, H. Yang, Z. Qiang, H. Pang, L. Sun, Z. Ma, R. Pate, A. Stiff-Roberts, S. Gao, J. Xu, G. J. Brown, W. Zhou, Colloidal quantum dot absorption enhancement in flexible Fano filters. *Appl. Phys. Lett.* **96**, 83111 (2010).
18. C. Goffaux, J. Sánchez-Dehesa, A. Levy Yeyati, Ph. Lambin, A. Khelif, J. O. Vasseur, B. Djafari-Rouhani, Evidence of Fano-like interference phenomena in locally resonant materials. *Phys. Rev. Lett.* **88**, 225502 (2002).
19. M. Junker, D. Dries, C. Welford, J. Hitchcock, Y. P. Chen, R. G. Hulet, Photoassociation of a Bose-Einstein condensate near a Feshbach resonance. *Phys. Rev. Lett.* **101**, 60406 (2008).
20. S. Inouye, M. R. Andrews, J. Stenger, H.-J. Miesner, D. M. Stamper-Kurn, W. Ketterle, Observation of Feshbach resonances in a Bose–Einstein condensate. *Nature* **392**, 151–154 (1998).
21. S. Giorgini, L. P. Pitaevskii, S. Stringari, Theory of ultracold atomic Fermi gases. *Rev. Mod. Phys.* **80**, 1215–1274 (2008).
22. F. Krausz, M. Ivanov, Attosecond physics. *Rev. Mod. Phys.* **81**, 163–234 (2009).
23. V. Gruson, L. Barreau, Á. Jiménez-Galan, F. Risoud, J. Caillat, A. Maquet, B. Carré, F. Lepetit, J.-F. Hergott, T. Ruchon, L. Argenti, R. Taïeb, F. Martín, P. Salières, Attosecond dynamics through a Fano resonance: Monitoring the birth of a photoelectron. *Science* **354**, 734–738 (2016).
24. A. Kaldun, A. Blättermann, V. Stooß, S. Donsa, H. Wei, R. Pazourek, S. Nagele, C. Ott, C. D. Lin, J. Burgdörfer, T. Pfeifer, Observing the ultrafast buildup of a Fano resonance in the time domain. *Science* **354**, 738–741 (2016).

25. A. Palacios, J. Feist, A. González-Castrillo, J. L. Sanz-Vicario, F. Martín, Autoionization of molecular hydrogen: Where do the Fano lineshapes go? *ChemPhysChem* **14**, 1456–1463 (2013).
26. J. A. R. Samson, G. N. Haddad, Total photoabsorption cross sections of H_2 from 18 to 113 eV. *J. Opt. Soc. Am. B* **11**, 277–279 (1994).
27. S. K. Semenov, N. A. Cherepkov, Generalization of the atomic RPA method for diatomic molecules: H_2 photoionization cross-section calculation. *Chem. Phys. Lett.* **291**, 375–380 (1998).
28. I. Sánchez, F. Martín, Resonant effects in photoionization of H2 and D2. *J. Chem. Phys.* **107**, 8391–8396 (1997).
29. C. J. Latimer, A. D. Irvine, M. A. McDonald, O. G. Savage, The dissociative photoionization of hydrogen via two-electron excitation at 27.5 eV and 30.5 eV. *J. Phys. B At. Mol. Opt. Phys.* **25**, L211–L214 (1992).
30. K. Ito, R. I. Hall, M. Ukai, Dissociative photoionization of H_2 and D_2 in the energy region of 25–45 eV. *J. Chem. Phys.* **104**, 8449–8457 (1996).
31. I. Sánchez, F. Martín, Origin of unidentified structures in resonant dissociative photoionization of H_2. *Phys. Rev. Lett.* **79**, 1654–1657 (1997).
32. C. J. Latimer, K. F. Dunn, F. P. O'Neill, M. A. MacDonald, N. Kouchi, Photoionization of hydrogen and deuterium. *J. Chem. Phys.* **102**, 722–725 (1995).
33. M. Glass-Maujean, S. Klumpp, L. Werner, A. Ehresmann, H. Schmoranzer, Photodissociation of doubly excited states of H_2 into H(2s) and H(2p) fragments. *J. Phys. B At. Mol. Opt. Phys.* **37**, 2677–2684 (2004).
34. J. D. Bozek, J. E. Furst, T. J. Gay, H. Gould, A. L. D. Kilcoyne, J. R. Machacek, F. Martín, K. W. McLaughlin, J. L. Sanz-Vicario, Production of excited atomic hydrogen and deuterium from H_2 and D_2 photodissociation. *J. Phys. B At. Mol. Opt. Phys.* **39**, 4871–4882 (2006).
35. L. Medišauskas, F. Morales, A. Palacios, A. González-Castrillo, L. Plimak, O. Smirnova, F. Martín, M. Yu Ivanov, Signatures of attosecond electronic–nuclear dynamics in the one-photon ionization of molecular hydrogen: Analytical model versus *ab initio* calculations. *New J. Phys.* **17**, 53011 (2015).
36. G. Sansone, F. Kelkensberg, J. F. Pérez-Torres, F. Morales, M. F. Kling, W. Siu, O. Ghafur, P. Johnsson, M. Swoboda, E. Benedetti, F. Ferrari, F. Lépine, J. L. Sanz-Vicario, S. Zherebtsov, I. Znakovskaya, A. L'Huillier, M. Y. Ivanov, M. Nisoli, F. Martín, M. J. J. Vrakking, Electron localization following attosecond molecular photoionization. *Nature* **465**, 763–766 (2010).
37. S. E. Canton, E. Plésiat, J. D. Bozek, B. S. Rude, P. Decleva, F. Martín, Direct observation of Young's double-slit interferences in vibrationally resolved photoionization of diatomic molecules. *Proc. Natl. Acad. Sci. U.S.A.* **108**, 7302–7306 (2011).
38. J. A. López-Domínguez, D. Hardy, A. Das, E. D. Poliakoff, A. Aguilar, R. R. Lucchese, Mechanisms of Franck–Condon breakdown over a broad energy range in the valence photoionization of N2 and CO. *J. Electron Spectros. Relat. Phenomena.* **185**, 211–218 (2012).
39. R. R. Lucchese, J. Söderström, T. Tanaka, M. Hoshino, M. Kitajima, H. Tanaka, A. De Fanis, J.-E. Rubensson, K. Ueda, Vibrationally resolved partial cross sections and asymmetry parameters for nitrogen *K* -shell photoionization of the N_2O molecule. *Phys. Rev. A* **76**, 12506 (2007).
40. E. Kukk, K. Ueda, U. Hergenhahn, X.-J. Liu, G. Prümper, H. Yoshida, Y. Tamenori, C. Makochekanwa, T. Tanaka, M. Kitajima, H. Tanaka, Violation of the Franck-Condon principle due to recoil effects in high energy molecular core-level photoionization. *Phys. Rev. Lett.* **95**, 133001 (2005).
41. K. Ueda, C. Miron, E. Plésiat, L. Argenti, M. Patanen, K. Kooser, D. Ayuso, S. Mondal, M. Kimura, K. Sakai, O. Travnikova, A. Palacios, P. Decleva, E. Kukk, F. Martín, Intramolecular photoelectron diffraction in the gas phase. *J. Chem. Phys.* **139**, 124306 (2013).
42. L. Argenti, T. D. Thomas, E. Plésiat, X.-J. Liu, C. Miron, T. Lischke, G. Prümper, K. Sakai, T. Ouchi, R. Püttner, V. Sekushin, T. Tanaka, M. Hoshino, H. Tanaka, P. Decleva, K. Ueda, F. Martín, Double-slit experiment with a polyatomic molecule: Vibrationally resolved C 1s photoelectron spectra of acetylene. *New J. Phys.* **14**, 33012 (2012).
43. I. Sánchez, F. Martín, Doubly excited autoionizing states of H_2 above the second ionization threshold: The Q_2 resonance series. *J. Chem. Phys.* **110**, 6702–6713 (1999).
44. I. Sánchez, F. Martín, The doubly excited states of the H2 molecule. *J. Chem. Phys.* **106**, 7720–7730 (1997).
45. L. D. Landau, E. M. Lifshitz, *Quantum Mechanics: Non-Relativistic Theory* (Oxford, ed. 3, 1977).
46. N. Berrah, B. Langer, A. A. Wills, E. Kukk, J. D. Bozek, A. Farhat, T. W. Gorczyca, High-resolution angle-resolved measurements in atoms and molecules using advanced photoelectron spectroscopy at the ALS. *J. Electron Spectros. Relat. Phenomena.* **101–103**, 1–11 (1999).
47. F. Martin, J. Fernández, T. Havermeier, L. Foucar, T. Weber, K. Kreidi, M. Schöffler, L. Schmidt, T. Jahnke, O. Jagutzki, A. Czasch, E. P. Benis, T. Osipov, A. L. Landers, A. Belkacem, M. H. Prior, H. Schmidt-Böcking, C. L. Cocke, R. Dörner, Single photon-induced symmetry breaking of H_2 dissociation. *Science* **315**, 629–633 (2007).
48. F. Martín, Ionization and dissociation using B-splines: Photoionization of the hydrogen molecule. *J. Phys. B At. Mol. Opt. Phys.* **32**, R197–R231 (1999).
49. H. Bachau, E. Cormier, P. Decleva, J. E. Hansen, F. Martín, Applications of B-splines in atomic and molecular physics. *Reports Prog. Phys.* **64**, 1815–1943 (2001).
50. A. Palacios, J. L. Sanz-Vicario, F. Martín, Theoretical methods for attosecond electron and nuclear dynamics: Applications to the H_2 molecule. *J. Phys. B At. Mol. Opt. Phys.* **48**, 242001 (2015).
51. J. Liu, E. J. Salumbides, U. Hollenstein, J. C. J. Koelemeij, K. S. E. Eikema, W. Ubachs, F. Merkt, Determination of the ionization and dissociation energies of the hydrogen molecule. *J. Chem. Phys.* **130**, 174306 (2009).

Acknowledgments: We thank M. Poullain for her help in producing fig. S1. **Funding:** This work was supported by European Research Council advanced grant 290853-XCHEM within the seventh framework program of the European Union. We also acknowledge the financial support from MINECO projects FIS2013-42002-R and FIS2016-77889-R, and the European COST (Cooperation in Science and Technology) Action XLIC CM1204, and the computer time from the Centro de Computación Científica de la Universidad Autónoma de Madrid and Marenostrum Supercomputer Center. A.P. acknowledges a Ramón y Cajal contract from the Ministerio de Economía y Competitividad (Spain). F.M. acknowledges support from the "Severo Ochoa" Programme for Centres of Excellence in R&D (MINECO, grant SEV-2016-0686) and the "María de Maeztu" Programme for Units of Excellence in R&D (MDM-2014-0377). S.E.C. acknowledges funding from the Helmoltz Recognition Award. The Extreme Light Infrastructure Attosecond Light Pulse Source project (GINOP-2.3.6-15-2015-00001) was financed by the European Union and cofinanced by the European Regional Development Fund. **Author contributions:** R.Y.B., A.P., M.Y.I., O.S., and F.M. developed the reconstruction model. R.Y.B., D.J., A.P., and F.M. performed the theoretical calculations and analyzed the theoretical results. S.E.C. designed the experiment and analyzed the experimental data. S.E.C., J.D.B., and B.R. performed the experiments. F.M. wrote the manuscript and coordinated the research. **Competing interests:** The authors declare that they have no competing interests. **Data and materials availability:** All data needed to evaluate the conclusions in the paper are present in the paper and/or the Supplementary Materials. Additional data related to this paper may be requested from the authors.

Submitted 22 February 2018
Accepted 18 July 2018
Published 24 August 2018
10.1126/sciadv.aat3962

Citation: R. Y. Bello, S. E. Canton, D. Jelovina, J. D. Bozek, B. Rude, O. Smirnova, M. Y. Ivanov, A. Palacios, F. Martín, Reconstruction of the time-dependent electronic wave packet arising from molecular autoionization. *Sci. Adv.* **4**, eaat3962 (2018).